

# Dynamic Stability of Elastomeric Bearings at Large Displacement

**A. Masroor, J. Sanchez, G. Mosqueda**  
*University at Buffalo, NY, USA*

**K. L. Ryan**  
*University of Nevada, Reno, USA*



## SUMMARY:

Bearings used in the seismic isolation of buildings can be subjected to large lateral deformations combined with high axial loads from overturning forces during strong shaking. Elastomeric bearing design requires an evaluation of the critical load capacity under this combined loading to ensure stability. To better understand and estimate the capacity of elastomeric bearings, dynamic stability tests were conducted on low damping natural rubber bearings. Although quasi-static testing of elastomeric bearings has been routine for more than a decade, the dynamic testing presented here was only attempted previously in a study of doweled bearings. In the experiments presented here, the stability of a rigid frame on four elastomeric bearings subjected to earthquake motions on a shake table is evaluated. These tests capture elastomeric bearing response at and beyond their stability limit under realistic loading conditions, providing unique data on the behavior of bolted elastomeric bearings at large displacements. Results from the dynamic stability test are compared to quasi-static test results and the reduced area formulation commonly used to predict the critical load of the elastomeric bearings.

*Keywords: Elastomeric bearing, dynamic stability, shake table simulator.*

## 1. INTRODUCTION

Past experimental and numerical studies have demonstrated the effectiveness of seismic isolation in reducing drifts and accelerations in buildings, thus reducing damage to structural and nonstructural elements. Seismic isolation is typically achieved by introducing bearing elements at the base of the structure with low horizontal and high vertical stiffness that decouple the superstructure from the effects of high frequency earthquake shaking. One type of commonly used isolator is the elastomeric bearing that consists of a number of alternating layers of rubber and steel shims bonded to produce a vertically stiff but horizontally flexible isolator. As a result of the added flexible interface to the structure, the isolators undergo large horizontal displacements that may lead to significant reduction in their critical axial load capacity. The critical load or stability limit in an elastomeric bearing is defined as the axial load for which the horizontal stiffness is reduced to zero.

Buckle and Kelly (1986) examined the experimental stability of modern seismic isolation bearings under quasi-static loading and dynamic loading wherein a scaled bridge on four doweled bearings was excited by a shaking table until the bearings overturned. The doweled bearings exhibit a rollover type of instability that differs from the expected behavior of bolted bearings examined here. Aiken et al. (1989) conducted an extensive experimental study of low shape factor elastomeric isolators by applying monotonically increasing axial load, with the top of the bearing free to displace horizontally. The tests

suggested that the response of the low shape factor bearings do not follow linear viscoelastic theory. The reduced area formulation is currently used in practice to determine the critical load in bearings and is presented in more detail later. Additional experiments on square bearings were conducted by Buckle et al. (2002) that further demonstrated the axial load capacity and lateral stiffness reduces with increasing horizontal displacement. Experimental results demonstrated that enough axial capacity exist at a lateral displacement equal to the bearing width and is not zero as estimated by design estimates used at the time. Extensive analytical and numerical studies have been performed to analyze the stability limit in elastomeric bearings and model their behavior. Koh and Kelly (1989) proposed a two-spring mechanical model and viscoelastic stability model based on bearing test results. A nonlinear analytical model was developed by Nagarajaiah and Ferrell (1999) based on the linear model by Koh and Kelly. The model satisfactorily predicted the nonlinear and post-stability limit behavior of elastomeric bearings of different sizes and shape factors for which experimental data was available (Buckle et al. 2002). Detailed nonlinear finite element (FE) analysis and an improved analytical formulation for predicting the reduced load carrying capacity of bearings based on a two-spring mechanical model was also presented by Weisman and Warn (2011).

This paper presents experimental results from four elastomeric bearings subjected to dynamic stability testing. The bearings tested are of reduced scale and relatively slender compared to those used in the seismic isolation of buildings and bridges. Dynamic stability testing using a shake table to apply dynamic loads to a rigid mass was conducted for the first time on four bolted bearings. The experimental results are compared to results obtained from quasi-static testing procedures on the same type of the bearing, as a means of evaluating the simpler quasi-static tests. In addition, these dynamic stability experiments support recent recommendations by Sanchez et al. (2012) on the use of revised parameters for the reduced area formulation commonly used to predict bearing stability for improved accuracy.

## 2. REDUCED AREA FORMULATION

Instability in elastomeric bearings can result from a reduction in the horizontal stiffness with increasing axial load. At the stability limit, the bearing is in equilibrium with the critical axial load and horizontal shear force, but has no additional lateral force capacity (horizontal stiffness is equal to zero). The reduced area formulation (Buckle and Liu 1994) has been shown to provide reasonably conservative estimates of the critical load for elastomeric bearings in the deformed configuration and is commonly used in practice to estimate the stability limit. The reduced area formula gives the critical load in the deformed configuration as:

$$P_{cr} = P_{cro} \left( \frac{A_r}{A} \right) \quad (2.1)$$

where  $A_r$ =the vertically overlapped area between the top and bottom of the bearing and  $A$  =total bearing area. The critical load at the undeformed configuration is defined as:

$$P_{cro} = \frac{\sqrt{G^2 A_s^2 + 4 G A_s P_e} - G A_s}{2} \quad (2.2)$$

where,

$$P_e = \frac{\pi^2 E_r I_s}{h^2}, \quad A_s = A \frac{h}{T_r}, \quad I_s = I \frac{h}{T_r} \quad (2.3)$$

$P_e$  is the Euler buckling load,  $G$  is the rubber shear modulus and  $A_s$  is the shear area.  $A$  and  $I$  are the area and moment of inertia of the bonded rubber area,  $T_r$  is the total rubber thickness,  $E_r$  is the rotational modulus and  $h$  is the total bearing height excluding the end plates. The shape factor ( $S$ ), defined as the ratio of the loaded area of rubber to the area of rubber free to bulge, is another important parameter related to the stability of elastomeric bearings.

### 3. EXPERIMENTAL PROGRAM

Dynamic experiments examining the stability of elastomeric bearings were conducted using the existing earthquake simulator at Network for Earthquake Engineering Simulation (NEES) Equipment Site at the University at Buffalo (UB). The test setup consisted of a rigid mass on four elastomeric bearings excited in only one horizontal direction.

#### 3.1. Description of Bearings

Four reduced scale elastomeric bearings were evaluated in this test program. Table 1 lists the elastomeric bearings geometric dimensions and material properties. Fig. 1 shows a schematic representation of the elastomeric bearings with the actual dimensions of the bearings listed in Table 1. Six nominally identical bearings were designed and manufactured for this testing program. Two of these bearings were dedicated for quasi-static testing (Sanchez et al. 2012) and the remaining 4 were subjected to the dynamic loading described here.

**Table 1. Properties of elastomeric bearing used in the test program.**

Description	Number of Bearings	Shape Factor	Height (mm)	D <sub>0</sub> (mm)	D <sub>i</sub> (mm)	A (mm <sup>2</sup> )	G <sub>eff</sub> (MPa) at 25 %	G <sub>eff</sub> (MPa) at 100 %	T <sub>r</sub> (mm)	N <sub>r</sub>
Natural Rubber	6	8.98	163.0	165	30	24129	0.6	0.46	3.17	25

#### 3.2. Dynamic Stability Tests

The dynamic stability tests used an earthquake simulator to investigate the dynamic behavior of rubber bearings at and beyond their stability limits under extreme ground motions. Although quasi-static testing of bolted elastomeric bearings has been routine for more than a decade, the dynamic testing presented here was only attempted previously in a study of doweled bearings exhibiting a rollover instability behavior (Buckle et al. 1986). The objective of these tests is to subject the bearings to more realistic loading conditions, allowing for better understanding of their behavior and capacity at the stability limit and to validate quasi-static stability test methods. The earthquake simulator setup simultaneously tested four bearings supporting approximately 231 kN, to provide a target vertical load on each bearing of 58 kN.

One of the twin earthquake simulators at the UB-NEES Equipment Site with a 50 metric ton payload capacity was used for the dynamic tests. The test setup, shown in Fig. 1, consists of a rigid block mounted on four elastomeric bearings excited in only one horizontal direction. The rigid block was constructed from a base steel frame supporting four steel plates and two concrete blocks for a combined load of 231

kN. A five-component load cell was located under each bearing to measure the axial force, shear force and moment during testing. Forty transducers measured the response of the rigid block model during the uni-directional dynamic tests, including two displacement transducers in the direction of testing, two in the out-of-plane direction and four in the vertical direction at each corner of the frame. Twelve accelerometers were installed to verify shear forces and moments obtained from load cells.

A series of dynamic characterization tests, including white noise, sinusoidal, and impulse motions, were first performed to characterize the dynamic properties of individual bearings and the isolated rigid block system. The impulse test was repeated after each earthquake simulation test to measure any changes in bearing properties. The model was subjected to a single horizontal component of three different ground motions at a range of intensities building up to Maximum Considerable Earthquake (MCE level). The ground motions listed in (Table 2) were selected from the Pacific Earthquake Engineering Research Center (PEER) database and were amplitude scaled by a factor that minimized the difference of the spectrum of the record and the MCE target spectrum in the least square sense from  $T = 0$  to 3 sec. The motions were also scaled in time by a factor of  $\frac{1}{2}$  for the assumed length scale factor of  $\frac{1}{4}$  (Masroor *et al.* 2012).

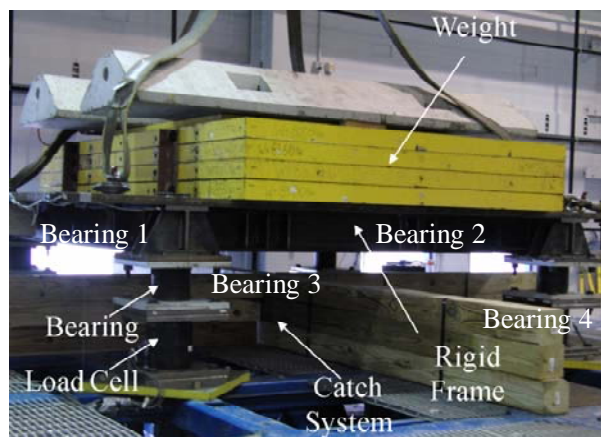


**Figure 1. Test setup for stability test Method 3**

**Table 2. List of ground motions and properties**

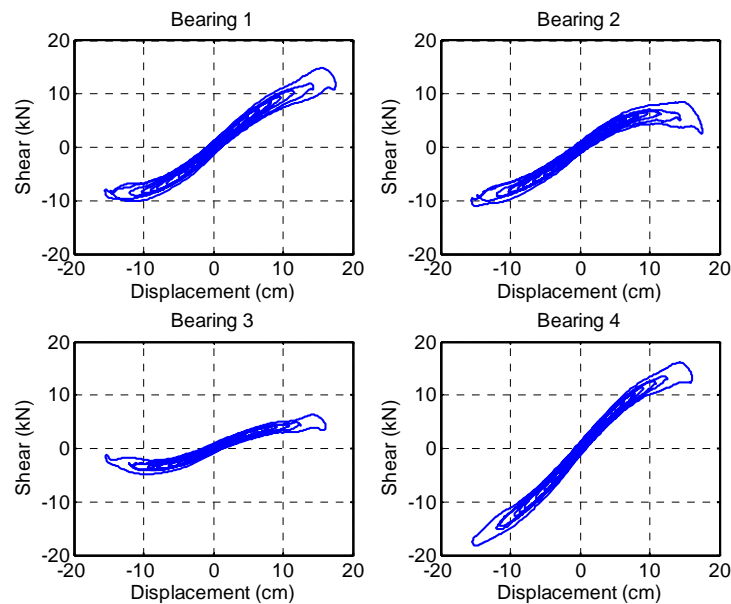
Ground Motion Record	Station	Magnitude (M)	MCE scale factor	Scaled PGA (g)	Duration (sec)
1994 Northridge - Newhall Fire Sta.	NWH360	6.69	1.46	0.86	40.0
1995 Kobe – Takatori	TAK090	6.90	0.89	0.55	40.9
1992 Erzincan – Erzincan Sta.	ERZ-NS	6.69	1.76	0.87	21.3

#### 4. EXPERIMENTAL RESULTS

The objective of dynamic stability testing was to experimentally investigate the stability limit of bearings under actual ground motions, and to compare these results with quasi-static tests (Sanchez *et al.* 2012). These earthquake simulations provide unique data on the behavior of bolted elastomeric bearings beyond their stability limit while subjected to realistic dynamic loading. For each earthquake record and amplitude, the time histories of horizontal displacement, axial load, and shear force were plotted for each bearing using the corresponding load cell data. Vertical and out-of-plane displacements were also

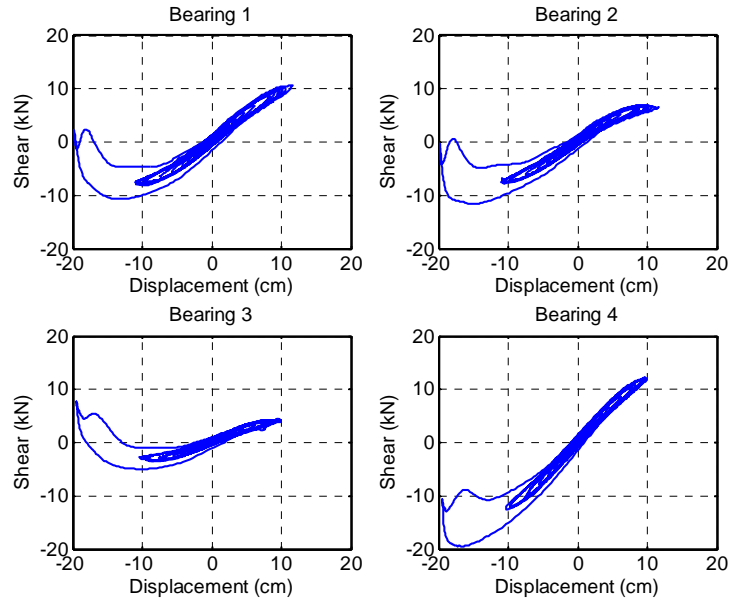
monitored to observe sudden changes at the stability limit. After each earthquake simulation test, an impulse identification test was executed to measure the stiffness and damping ratio in each bearing. Fig. 1 indicates the location of each bearing in the test setup and the direction of earthquake loading. Due to minor misalignments, the gravity load was not evenly distributed between the four bearings. Thus, two bearings on the same side of the frame exhibited different hysteretic behavior.

Figs. 2 and 3 show the dynamic response of each bearing subjected to 67% and 85% of MCE level of the Erzincan ground motion, respectively. One or more stability limits can be identified in the shear force-displacement plots of each bearing where the force peaks and the stiffness is zero in each loop. It is evident that the stability limit was achieved in several cycles during the same ground motion, with occurrences at different displacements and shear forces due to the variation of axial load during testing. The largest displacements in the bearings were observed for 85% Erzincan record shown in Fig. 3. In this case, Bearing 3 sustained displacements 90% beyond their stability limit with substantial strength degradation combined with P- $\Delta$  forces at large displacements.

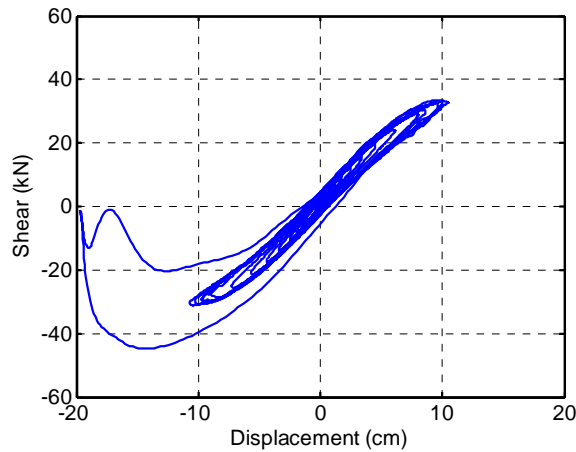


**Figure 2. Bearing hysteresis loop under 67% MCE level of Erzincan record**

Fig. 4 presents the total base shear hysteresis loop for the structure under 85% of MCE level Erzincan record, obtained by summing the shear force in all four bearings and considering the displacement at the center of mass. While the composite stiffness of the isolators appears negative and thus indicating post stable behavior, the total resisting force only approached zero and did not reverse signs under increasing displacements as was the case for the individual Bearing 3. As indicated from the hysteresis loops, the isolators were able to recover and re-center after each excursion beyond the stability limit. This observation may be highly dependent on the instantaneous dynamic response of the system and characteristics of the ground motion.

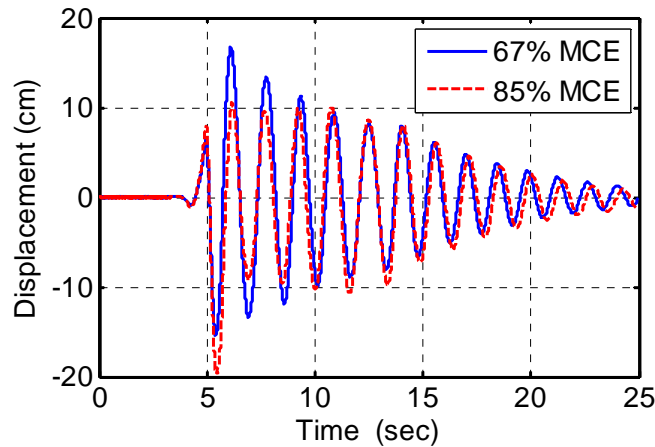


**Figure 3. Bearing hysteresis loop under 85% MCE level of Erzincan record**



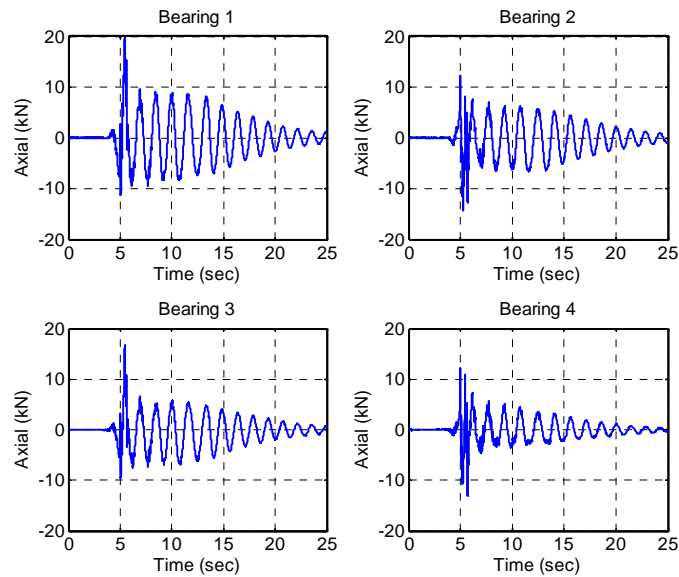
**Figure 4. Total base shear hysteresis loop under 85% MCE level of Erzincan record**

Fig. 5 shows the isolators displacement at 67 and 85% of MCE level of Erzincan record. It can be seen that by increasing the amplitude in input motion, larger displacement occurs in first peak leading to instability in all bearings shown in Fig. 4. This instability in bearings which is clear by negative stiffness in Fig. 4 leads to smaller displacement in next cycles of the bearing. For example in second cycle maximum displacement decreased to 10 cm that was 15 cm at 67% of MCE level. This decreasing in displacement prevents occurring another instability situation in bearing in positive displacement. This positive instability that was initiated at 67% of MCE level (Fig. 3) was prevented by reaching the stability limit in bearings in negative displacement.



**Figure 5. Bearing displacement under 67 and 85% MCE level of Erzincan record**

Fig. 6 shows axial force variation for each bearing under 85% MCE level of Erzincan record. It is important to mention that static load was removed from these figures. Moving the mass plate in the negative displacement leads to increasing axial load in bearings 1 and 3 and decreasing axial load on bearings 2 and 4. Maximum variation of 20 kN was observed at the instant of stability limit at bearing displacement of 20 cm (120% of bearing diameter), which is approximately 35% of initial axial load.



**Figure 6. Axial force variation for each bearing under 85% MCE level of Erzincan record**

Table 3 lists the tests conducted and includes – for each bearing that reached its stability limit – the ratio of the maximum displacement to the displacement at the corresponding stability limit in the same loading cycle. For the 85% of MCE level Takatori record, the stability limit was observed only in Bearing 3 and the maximum displacement in Bearing 3 was 1.39 times the stability limit displacement. The Erzincan motion was not attempted at 100% MCE amplitude due to the large displacements observed under 85% MCE amplitude.

**Table 3. Ratio of maximum displacement to point of instability for each isolator at different ground motion intensities**

Bearing	67% MCE			85% MCE			100% MCE		
	Newhall	Takatori	Erzincan	Newhall	Takatori	Erzincan	Newhall	Takatori	Erzincan
1	-*	-	1.15	-	-	1.42	1.25	1.24	NA
2	-	-	1.17	-	-	1.31	1.17	1.24	NA
3	-	-	1.55	-	1.39	1.94	1.38	1.53	NA
4	-	-	1.14	-	-	1.16	1.12	-	NA

\* Bearing did not reach instability limit

To compare the stability limits obtained from the dynamic tests with quasi-static tests conducted on the same type of the bearing (Sanchez *et al.* 2012), Fig. 7 plots the experimentally determined critical load from both methods. The two experimental methods clearly provide similar results. Due to limitations in testing, the dynamic stability limits are concentrated at large displacements with lower axial loads while those determined by quasi-static testing are more evenly distributed across the displacement range. The critical load approximations based on the reduced area formulation (Eqn. 2.1) using  $G_{eff}$  at 25% and 100% shear strain were also plotted to compare with dynamic stability results. To calculate the shear modulus, the average of the four bearings was used.

The reduced area formulation is dependent on the critical load at the undeformed configuration,  $P_{cro}$ , typically estimated using Eqn. 2.2 with  $G_{eff}$  at 100% shear strain. Sanchez *et al.* (2012) show that the estimate of the critical load in the undeformed configuration (Eqn 2.2) can be improved by using the effective shear modulus at a smaller shear strain. Use of  $G_{eff}$  at 25% strain more closely approximates dynamic tests results, although the experimental results suggest significant critical load capacity is present at displacements equal to the bearing diameter. It is important to note that  $G_{eff}$  at 100% shear strain provides reasonable conservative estimates for critical load design, but use of  $G_{eff}$  at 25% can provide more accurate predictions.

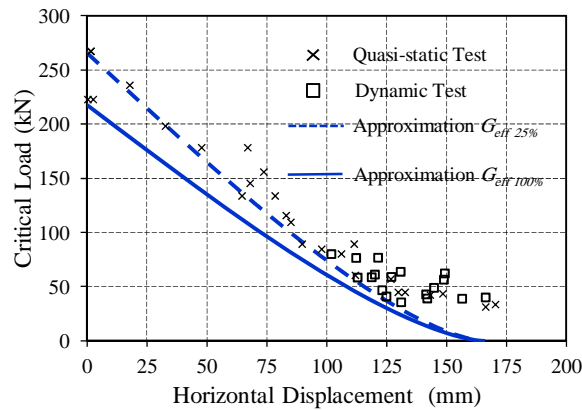


**Figure 7. Quasi-static and dynamic stability test results**

## 5. MONITORING OF BEARING PROPERTIES

Characterization tests were conducted intermittently throughout the test program to monitor changes in the mechanical properties of the bearings. Impulse excitation tests at amplitude of 0.1g and frequency equal to resonant frequency of the isolated structure were conducted throughout the shake table tests.

Fig. 8 shows the measured response of Bearing 3 during six impulse tests conducted after each of the dynamic stability method test. Approximately 13% increase in the damping ratio and 10% decrease in the effective shear modulus were observed over the course of the tests, indicating that the bearing properties remained relatively constant in these bearings. The largest change in both parameters occurred after the Erzincan motion at 85% of MCE amplitude, which resulted in peak displacement that was 1.94 times greater than the displacement at the stability limit.

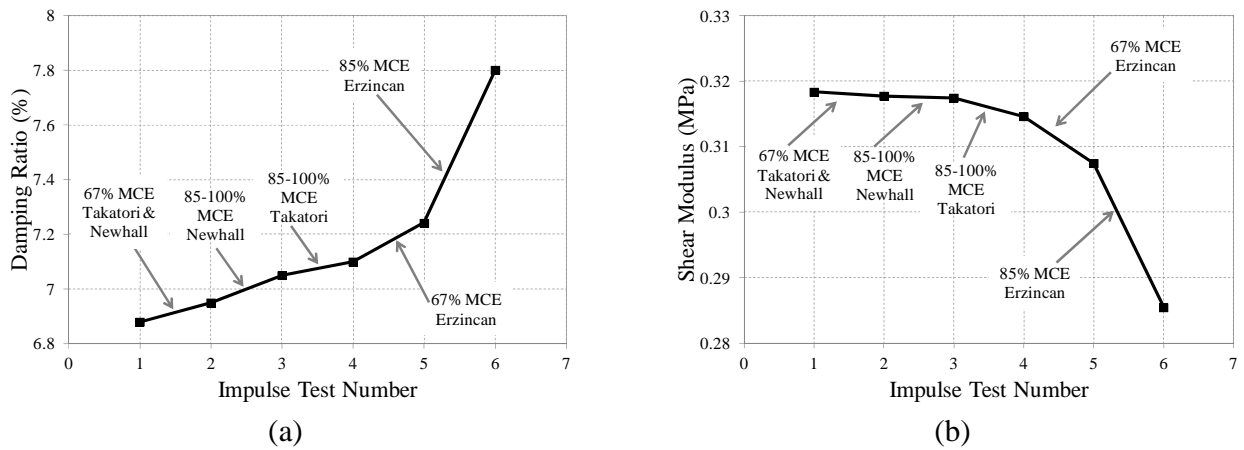


**Figure 8. Benchmark tests results for dynamic stability method (a) damping ratio and (b) average shear modulus**

## 6. CONCLUSION

A seismically isolated rigid frame model was subjected to a single horizontal component of various ground motions at a range of scaled amplitudes until the stability limit was reached. The dynamic stability tests demonstrate that elastomeric bearings can perform well and recover from excursions beyond the stability limit without seemingly negative consequences to the structural system. However, these observations are based on limited testing and can depend on the characteristics of the ground motion as well as the amount of axial load variation. Results from the dynamic stability test are compared to available quasi-static test results for the same type of the bearing and the reduced area formulation commonly used to predict the critical load of the elastomeric bearings. Results from dynamic tests and quasi-static agree well, confirming that the simpler quasi-static method is effective to experimentally determine the stability limit of elastomeric bearings. The test data show that at large horizontal displacements, equal to the diameter of the bearing, the bearing can sustain over 15% of the critical load in the undeformed configuration although the reduced area formulation predicts zero load capacity. Based on the stability test results and the predicted stability curves in Fig. 7 the critical load can be predicted with improved accuracy by the reduced area formula based on  $G_{eff}$  at 25% shear strain compared to  $G_{eff}$  at 100% shear strain as typically used in design.

## ACKNOWLEDGEMENT

This work is part of the NEES TIPS project supported by the National Science Foundation (NSF) under Grants No. CMMI-0724208 and CMMI-1113275. Any opinions, findings, conclusions or recommendations expressed in this document are those of the investigators and do not necessarily reflect the views of NSF. The authors are grateful to Drs. M. Constantinou and A. Whittaker for the helpful discussion and advice provided throughout this study.

## REFERENCES

- Aiken, I. D., Kelly, J. M., Tajirian, F. F., (1989). “Mechanics of low shape factor elastomeric seismic isolation bearings.” *UCB/EERC-89/13*, Earthquake Engineering Research Center, University of California at Berkeley, CA.
- Buckle, I. G., and Kelly, J. M. (1986). “Properties of slender elastomeric isolation bearings during shake table studies of a large-scale model bridge deck.” *Joint Sealing and bearing systems for concrete structures*, ACI, Detroit, Mich., **Vol. 1**, 247–269.
- Buckle, I. G., and Liu, H. (1994). “Experimental determination of critical loads of elastomeric isolators at high shear strain.” *NCEER Bulletin*, **8(3)**, 1–5.
- Buckle, I., Nagarajaiah, S., and Ferrell, K. (2002), “Stability of Elastomeric Isolation Bearings: Experimental Study”, *Journal of Structural Engineering*, **128(1)**, 3-11.
- Koh, C. G., and Kelly, J. M. (1989). “Viscoelastic stability model for elastomeric isolation bearings.” *Journal of Structural Engineering*, **115(2)**, 285–302.
- Nagarajaiah, S., and Ferrell, K. (1999). “Stability of elastomeric seismic isolation bearings.” *Journal of Structural Engineering*, **125(9)**, 946-954.
- Masroor, A., Mosqueda, G. (2012). “Experimental simulation of base-isolated buildings pounding against moat wall and effects on superstructure response.” *Earthquake Engineering and Structural Dynamic*, DOI: 10.1002/eqe.2177.
- Sanchez, J., Masroor, A., Mosqueda, G., Ryan, K. (2012), “Static and Dynamic Stability of Elastomeric Bearings for Seismic Protection of Structures”, *Journal of Structural Engineering*, In Review.
- Weisman J, Warn GP. (2011). “Stability of Elastomeric and Lead-Rubber Seismic Isolation Bearings.” *Journal of Structural Engineering*, **1**:345-345.